Inorg. Chem. **2005**, *44*, 572–583

Formate—The Analogue of Azide: Structural and Magnetic Properties of $M(HCOO)_2(4,4'\text{-bpy})\cdot nH_2O$ (M = Mn, Co, Ni; n = 0, 5)

Xin-Yi Wang, Hai-Yan Wei, Zhe-Ming Wang, Zhi-Da Chen,* and Song Gao*

State Key Laboratory of Rare Earth Materials Chemistry and Applications & PKU-HKU Joint Laboratory on Rare Earth Materials and Bioinorganic Chemistry, College of Chemistry and Molecular Engineering, Peking University, Beijing 100871, People's Republic of China

Received June 25, 2004

Reaction of transition metal formate $M(HCOO)_2\cdot 2H_2O$ (M = Mn, Co, Ni) with 4,4′-bpy (4,4-bipyridine) has led to four new compounds with the formula $M(HCOO)_2(4,4'\text{-bpy})\cdot nH_2O$ (M = Mn, Co (**1·Mn**, **2·Co**), n = 0; M = Co, Ni (**3·Co**, **4·Ni**), n = 5). Compounds **1·Mn** and **2·Co** are isomorphous and crystallized in the tetragonal crystal system with the chiral space group $P4_12_12$. They are of three-dimensional diamondoid structure connected by *anti–anti* formate with 4,4′-bpy in the cavities of the framework reinforcing the intermetallic connections; the diamond-like net was observed also in their azide analogue ($Mn(N_3)_2(4,4'\text{-bpy})$). Compounds **3·Co** and **4·Ni** are isomorphous also but crystallized in the monoclinic crystal system with the space group *Cc*. Both structures are uninterpenetrated 3D "$CdSO_4$" type with big channels, constructed by *anti–anti* formate and 4,4′-bpy. This type of net was not observed in their azide analogue. Residing in the channels, water molecules form a new type of 1D tape constructed by vertex-sharing cyclic pentamers. Magnetic measurements were performed on all of these four compounds. **1·Mn** and **2·Co** are weak ferromagnets with the critical temperature T_c = 5.3 and 7.4 K, respectively. **3·Co** is an antiferromagnet with Néel temperature T_N = 3.0 K, and **4·Ni** is a weak ferromagnet below 20 K. Hysteresis loop can be observed for **2·Co** and **4·Ni** at 1.8 K. As an analogue of azide, formate can be used to construct molecular architectures, which structurally and magnetically have great similarities to and also differences from those of azide. This offers a promising method for the design of new molecular architectures with formate.

Introduction

Molecule-based magnetic polymers have attracted intense interest in recent years, due to not only the fundamental research of magnetic interactions and magneto-structural correlations, but also the development of new functional molecule-based materials.[1] The rational design of these polymers remains to be one of the major challenges. The main emphasis on the principle of design is to search for good bridging ligands that can effectively mediate the magnetic coupling between the local spin carriers. During the past several decades, the bridging ligands including CN^-, N_3^-, $C_2O_4^{2-}$, $N(CN)_2^-$, and carboxyl groups have been widely investigated, and numerous compounds bridged by these ligands have been reported. Among them, azide ion was the all-important one, if not the most, because of the abundant bridging modes and the ability to mediate strong magnetic coupling, either ferro- or antiferromagnetic.[2] However, the poisonous character and the high possibility to explode may disable azide for further applications in the future. So, there appears the question: are there any other analogues of azide to construct magnetic coordination polymers? Formate ion is a rational choice. As the smallest carboxylate, the formate ion has been observed to display multiple bridging modes (Scheme 1) such as the common 2.11, the frequent 3.21, and the unusual 4.22 mode[3] to link

* Authors to whom correspondence should be addressed. E-mail: gaosong@pku.edu.cn (S.G.); zdchen@pku.edu.cn (Z.-D.C.).

(1) (a) Sato, O.; Iyoda, T.; Fujishima, A.; Hashimoto, K. *Science* **1996**, *272*, 704. (b) Kahn, O.; Martinez, C. J. *Science* **1998**, *279*, 44. (c) Gütlich, P.; Garcia, Y.; Woike, T. *Coord. Chem. Rev.* **2001**, *219–221*, 839. (d) Niel, V.; Thompson, A. L.; Muñoz, C.; Galet, A.; Goeta, A. E.; Real, J. A. *Angew. Chem.* **2003**, *115*, 3890–3893; *Angew. Chem., Int. Ed.* **2003**, *42*, 3760–3763.

(2) (a) Ribas, J.; Escuer, A.; Monfort, M.; Vicente, R.; Cortés, R.; Lezama, L.; Rojo, T. *Coord. Chem. Rev.* **1999**, *193–195*, 1027–1078. (b) Gao, E.-Q.; Yue, Y.-F.; Bai, S.-Q.; He, Z.; Yan, C.-H. *J. Am. Chem. Soc.* **2004**, *126*, 1419–142. (c) Liu, T.-F.; Fu, D.; Gao, S.; Zhang, Y.-Z.; Sun, H.-L.; Su, G.; Liu, Y.-J. *J. Am. Chem. Soc.* **2003**, *125*, 13976.

(3) Harris notation: Harris notation describes the binding mode as $[X\cdot Y_1Y_2Y_3...Y_n]$, where X is the overall number of metals bound by the whole ligand, and each value of Y refers to the number of metal atoms attached to the different donor atoms. The ordering of Y is listed by the Cahn–Ingold–Prelog priority rules.

10.1021/ic049170t CCC: $30.25
Published on Web 01/13/2005

Scheme 1 The Bridging Mode for μ-$HCOO^-$ and μ-N_3^-

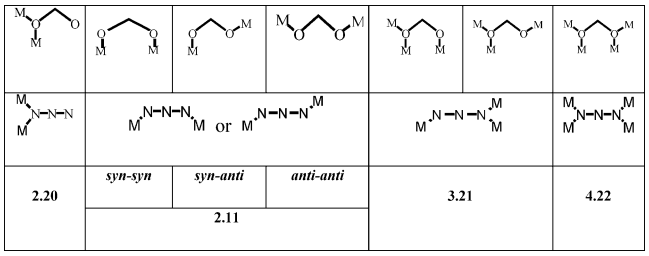

two or more transition-metal ions forming a variety of zero-,[4−6] one-,[7] two-,[8] and three-dimensional[9−12] complexes. Depending on the geometry characters of formate and the metal ions, formate can adopt different bridging modes such as *syn*−*syn*, *anti*−*anti*, *syn*−*anti*, and monatomic, and they mediate ferro- or antiferromagnetic coupling between metal ions in different situations.[9−12] Interestingly, all of these bridging modes can find their corresponding ones in azide compounds (see also Scheme 1). The magnetic coupling transferred by formate or azide ion is also of some similarity. For example, both with the 2.20 mode can mediate ferro- or antiferromagnetic interactions depending on the angle of M−O(N)−M, and those with the 2.11 mode can always mediate antiferromagnetic coupling. These similarities may lead to compounds with similar structures and magnetic properties. At the same time, due to the differences in coordination atoms (O or N), electronic structures (degree of conjugating), and the geometric characters (bended or linear) of these two ions, the structures and the magnetic properties containing these two anions are not always the same. As an example, N_3^- can usually mediate stronger magnetic coupling than does formate, thus leading to higher magnetic transition temperatures.[13]

Many compounds containing formate as bridging ligand have been analyzed in structure and magnetism.[8−11,13a,b] The simple isomorphous metal formate $M(HCOO)_2{\cdot}2H_2O$ (M = Mn, Fe, Co, Ni, Cu)[11] and their anhydrates $M(HCOO)_2$ (M = Mn, Cu),[10] $M(HCOO)_2{\cdot}2(NH_2)_2CO$ (M = Mn, Co),[8b,c] $Mn^{III}(HCOO)_3{\cdot}{}^1/_2CO_2{\cdot}{}^1/_4HCOOH{\cdot}{}^2/_3H_2O$,[9c] $Co(HCOO)_2(HCONH_2)_2$,[8a] and $Mn_3(HCOO)_6{\cdot}G$ (G = guests)[9a] and our very recent results on $M(HCOO)_3[NH_2(CH_3)_2]$ (M = Mn, Co, Ni)[13a,b] all show long-range magnetic ordered states. As compared to the very similar compound $Mn(N_3)_3[N(CH_3)_4]$,[13c,d] $M(HCOO)_3[NH_2(CH_3)_2]$ ordered at lower temperatures, but they give us a clue to further investigate other formates with a second bridging ligand to see the similarity and the difference between formates and azides. With this idea in mind, we investigated a number of formates with a second bridging ligand such as 4,4′-bpy, *trans*-4,4′-azobis(pyridine), and so on. To the best of our knowledge, the only example of formate complex with 4,4′-bpy is the paramagnetic $Cu(HCOO)_2(4,4'\text{-bpy})$,[9b] reported by J. L. Manson very recently. Here, we report the syntheses, crystal structures, and magnetic properties of a series of metal formates with the formula $M(HCOO)_2(4,4'\text{-bpy}){\cdot}nH_2O$ (M = Mn, Co (**1·Mn**, **2·Co**), $n = 0$; M = Co, Ni (**3·Co**, **4·Ni**), $n = 5$). Among them, **1·Mn** and **2·Co** have the same diamondoid structure as $Cu(HCOO)_2(4,4'\text{-bpy})$ and their azide analogue $Mn(N_3)_2(4,4'\text{-bpy})$[14] and show spin-canted weak ferromagnetism with the critical temperature $T_c = 5.3$ and 7.4 K, respectively. For **1·Mn**, **a** spin-flop transition occurs upon application of a critical field $H_{SF} = 5.75$ kOe. **3·Co** and **4·Ni** are different

(4) (a) Youngme, S.; Somjitsripunya, W.; Chinnakali, K.; Chantrapromma, S.; Fun, H. K. *Polyhedron* **1999**, *18*, 857. (b) Norman, R. E.; Leising, R. A.; Yan, S.-P.; Que, L. *Inorg. Chim. Acta* **1998**, *273*, 393−396. (c) Escrivà, E.; Carrió, J. S.; Lezama, L.; Folgado, J. V.; Pezarro, J. L.; Ballesteros, R.; Abarca, B. *J. Chem. Soc., Dalton Trans.* **1997**, 2033−2038. (d) Brooker, S.; Mckee, V.; Metcalfe, T.; *Inorg. Chim. Acta* **1996**, *246*, 171. (e) Sapiña, F.; Burgos, M.; Escrivá, E.; Folgado, J. V.; Beltrán, D. *Inorg. Chim. Acta* **1994**, *216*, 185−190. (f) Sessler, J. L.; Hugdahl, J. D.; Lynch, V.; Davis, B. *Inorg. Chem.* **1991**, *30*, 334. (g) Yamanaka, M.; Uekusa, H.; Ohba, S.; Saito, Y.; Iwata, S. *Acta Crystallogr.* **1991**, *B47*, 344−355. (h) Armstrong, W. H.; Spool, A.; Papaefthymiou, G. C.; Frankel, R. B.; Lippard, S. J. *J. Am. Chem. Soc.* **1984**, *106*, 3653. (i) Cotton, F. A.; Rice, G. W. *Inorg. Chem.* **1978**, *17*, 688−692.

(5) (a) Boyle, T. J.; Alam, T. M.; Tafoya, C. J.; Scott, B. L. *Inorg. Chem.* **1998**, *37*, 5588. (b) Scott, M. J.; Goddard, C. A.; Holm, R. H. *Inorg. Chem.* **1996**, *35*, 2558−2567.

(6) Cadiou, C.; Coxall, R. A.; Graham, A.; Harrison, A.; Helliwell, M.; Parsons, S.; Winpenny, R. E. P. *Chem. Commun.* **2002**, 1106−1107.

(7) (a) Sanchis, M. J.; Gómez-Romero, P.; Folgado, J. V.; Sapiñaz, R.; Beltrán, A.; García, J.; Beltrán, D. *Inorg. Chem.* **1992**, *31*, 2915. (b) Turner, P.; Gunter, M. J.; Hambley, T. W.; White, A. H.; Skelton, B. W. *Inorg. Chem.* **1992**, *31*, 2297−2299. (c) Lis, T.; Trzebiatowska, B. J. *Acta Crystallogr.* **1977**, *B33*, 2112−2116.

(8) (a) Rettig, S. J.; Thompson, R. C.; Trotter, J.; Xia, S. H. *Inorg. Chem.* **1999**, *38*, 1360−1363. (b) Kubo, H.; Zenmyo, K.; Matsumura, M.; Takeda, K.; Alhara, K.; Yamagata, K. *J. Phys. Soc. Jpn.* **1999**, *68*, 253−257. (c) Fujino, M.; Achiwa, N.; Koyano, N.; Shibuya, I.; Ridwan; Yamagata, K. *J. Magn. Magn. Mater.* **1992**, *104*−*107*, 851−852.

(9) (a) Wang, Z.-M.; Zhang, B.; Fujiwara, H.; Kobayashi, H.; Kurmoo, M. *Chem. Commun.* **2004**, 416−417. (b) Manson, J. L.; Lecher, J. G.; Gu, J.-Y.; Geiser, R.; Schlueter, J. A.; Henning, R.; Wang, X.-P.; Schultz, A. J.; Koo, H. J.; Whangbo, M. H. *J. Chem. Soc., Dalton Trans.* **2003**, 2905−2911. (c) Cornia, A.; Caneschi, A.; Dapporto, P.; Faberetti, A. C.; Gatteschi, D.; Malevasi, W.; Sangregorio, C.; Sessoli, R. *Angew. Chem.* **1999**, *111*, 1897−1899; *Angew. Chem., Int. Ed.* **1999**, *38*, 1780−1781.

(10) (a) Viertelhaus, M.; Henke, H.; Anson, C. E.; Powell, A. K. *Eur. J. Inorg. Chem.* **2003**, 2283−2289. (b) Sapiña, F.; Burgos, M.; Escrivá, E.; Folgado, J. V.; Marcos, D.; Beltrán, A.; Beltrán, D. *Inorg. Chem.* **1993**, *32*, 4337−4334.

(11) (a) Kageyama, H.; Khomskii, D. I.; Levitin, R. Z.; Vasil'ev, A. N. *Phys. Rev. B* **2003**, *67*, 224422. (b) Radhakrishnatt, P.; Gillonf, B.; Chevrierts, G. *J. Phys.: Condens. Matter* **1993**, *5*, 6147. (c) Takeda, K.; Kawasaki, K. *J. Phys. Soc. Jpn.* **1971**, *31*, 1026. (d) Burlet, P.; Burlet, P.; Bertaut, E. F.; Roult, G.; Pillon, J. *J. Solid State Commun.* **1969**, *7*, 1403−1408. (e) Yamagata, K. *J. Phys. Soc. Jpn.* **1967**, *22*, 582−589. (f) Okada, K.; Kay, M. I.; Cromer, D. T.; Almodovar, I. *J. Chem. Phys.* **1966**, *44*, 1648. (g) Hoy, G. R.; Barros, S. De S.; Barros, F. De S.; Friedberg, S. A. *J. Appl. Phys.* **1965**, *36*, 936. (h) Wagner, G. R.; Friedberg, S. *Appl. Phys. Lett.* **1964**, *9*, 11. (i) Martin, R. L.; Waterman, H. *J. Chem. Soc.* **1959**, 1359.

(12) (a) Kaufman, A.; Afshar, C.; Rossi, M.; Zacharias, D. E.; Glusker, J. P. *Struct. Chem.* **1993**, *4*, 191. (b) Bird, M. J.; Lomer, T. R. *Acta Crystallogr.* **1971**, *B27*, 859. (c) Kay, M. I.; Almodovar, I.; Kaplan, S. F. *Acta Crystallogr.* **1968**, *B24*, 1312−1316. (d) Okada, K.; Kay, M. I.; Kromer, D. T.; Almodovar, I. *J. Chem. Phys.* **1966**, *44*, 1648. (e) Strzyżewska, M. B. *Acta Crystallogr.* **1965**, *19*, 357−362. (f) Krogmann, V. K.; Mattes, R. *Z. Kristallogr.* **1963**, *118*, 291−302. (g) Barclay, G. A.; Konnard, C. G. L. *J. Chem. Soc.* **1961**, 3289. (h) Kiriyama, R.; Ibamoto, H.; Matsuo, K. *Acta Crystallogr.* **1954**, *7*, 482.

(13) (a) Wang, X.-Y.; Gan, L.; Zhang, S.-W.; Gao, S. *Inorg. Chem.* **2004**, *43*, 4615−4625. (b) Wang, Zh.-M.; Zhang, B.; Takeo, O.; Katsuya, I.; Hayao, K.; Mohamedally, K. *J. Chem. Soc., Dalton Trans.* **2004**, 2209−2216. (c) Mautner, F. A.; Hanna, S.; Cortés, R.; Lezama, L.; Barandika, M. G.; Rojo, T. *Inorg. Chem.* **1999**, *38*, 4647−4652. (d) Mautner, F.; Cortés, A. R.; Lezama, L.; Rojo, T. *Angew. Chem.* **1996**, *108*, 96; *Angew. Chem., Int. Ed. Engl.* **1996**, *35*, 78.

(14) (a) Han, S.; Manson, J. L.; Kim, J.; Miller, J. S. *Inorg. Chem.* **2000**, *39*, 4182−4185. (b) Martín, S.; Barandika, M. G.; Lezama, L.; Pizarro, J. L.; Serna, Z. E.; De Larramendi, J. I. R.; Arriortua, M. I.; Rojo, T.; Cortés, R. *Inorg. Chem.* **2001**, *40*, 4109−4115.

Table 1. Crystallographic Data for Compounds **1**−**4**

	1·Mn	**2·Co**	**3·Co**	**4·Ni**
formula	$C_{12}H_{10}N_2O_4Mn$	$C_{12}H_{10}N_2O_4Co$	$C_{12}H_{20}N_2O_9Co$	$C_{12}H_{20}N_2O_9Ni$
M_r [g mol^{-1}]	301.16	305.15	395.23	395.01
crystal system	tetragonal	tetragonal	monoclinic	monoclinic
space group	$P4_12_12$	$P4_12_12$	Cc	Cc
a [Å]	8.1469 (2)	7.9861 (2)	10.5108 (3)	10.4815 (2)
b [Å]	8.1469 (2)	7.9861 (2)	20.2765 (7)	20.0601 (4)
c [Å]	17.8046 (5)	17.4996 (5)	8.1309 (2)	8.1266 (2)
α [deg]	90	90	90	90
β [deg]	90	90	102.223 (2)	102.633 (9)
γ [deg]	90	90	90	90
V [Å^3]	1181.73 (5)	1116.07 (5)	1693.59(9)	1667.33(6)
Z	4	4	4	4
ρ_{calcd} [g cm^{-3}]	1.693	1.816	1.550	1.574
crystal size [mm^{-1}]	0.5 × 0.4 × 0.3	0.3 × 0.3 × 0.15	0.3 × 0.3 × 0.15	0.4 × 0.3 × 0.15
μ(Mo Kα) [mm^{-1}]	1.128	1.550	1.061	1.212
measured refl.	14 195	21 172	14 247	15 761
independent refl.	1358	1286	3774	3820
observed refl.[a]	1052	1032	3048	3245
no. parameters	90	90	219	288
F(000)	612	620	820	824
GOF	0.961	0.945	0.998	0.959
max/min (e Å^{-3})	0.221/−0.175	0.224/−0.262	0.510/−0.489	0.268/−0.562
T_{max}/T_{min}	0.720/0.670	0.795/0.682	0.857/0.819	0.837/0.708
R1[b]	0.0243	0.0255	0.0352	0.0279
wR2[c]	0.0473	0.0503	0.0784	0.0609

[a] Observation criterion: $I > 2\sigma(I)$. [b] $R1 = \sum||F_o| - |F_c||/\sum|F_o|$; $I > 2\sigma(I)$. [c] $wR2 = \{\sum[w(F_o^2 - F_c^2)^2]/\sum[w(F_o^2)^2]\}^{1/2}$, for all data.

from the corresponding azide compounds, and they both crystallized as a novel noninterpenetrated "$CdSO_4$" type structure with big channels. Residing in the channels, water molecules form novel 1D tapes constructed by vertex-sharing cyclic pentamers. **3·Co** is an antiferromagnet with Neel temperature $T_N = 3.0$ K and has complex spin-flop transitions, while **4·Ni is** a weak ferromagnet below 20 K.

Experimental Section

General Remarks. All starting materials were commercially available, reagent grade, and used as purchased without further purification. $M(HCOO)_2{\cdot}2H_2O$ (M = Mn, Co) was prepared by reaction of MCO_3 with formate, and $Ni(HCOO)_2{\cdot}2H_2O$ was purchased from E. Merck. Elemental analyses of carbon, hydrogen, and nitrogen were carried out with an Elementary Vario EL. The micro-infrared spectroscopy studies were performed on a Magna-IR 750 spectrophotometer in the 4000−500 cm^{-1} region. Thermogravimetric analyses (TGA) were performed on a Du Pont 1090B thermal analyzer. Variable-temperature magnetic susceptibility, zero-field ac magnetic susceptibility measurements, and field dependence of magnetization were performed on an Oxford Maglab 2000 System or a Quantum Design MPMS XL-5 SQUID system. The experimental susceptibilities were corrected for the diamagnetism of the constituent atoms (Pascal's tables).

Synthesis. $Mn(HCOO)_2$(4,4′-bpy) (1·Mn). $Mn(HCOO)_2{\cdot}2H_2O$ (0.5 mmol) dissolved in 10 mL of hot water was added to 10 mL of DMF (DMF = *N*,*N*-dimethylformamide) solution containing 0.5 mmol of 4,4′-bpy. Some precipitates were formed immediately and dissolved by heating the solution to about 100 °C. The filtrated solution was left undisturbed at room temperature. Slow evaporation of the solution gave fine pale yellow block crystals in 2 weeks, yield 60%. Anal. (%) Calcd for $C_{12}H_{10}N_2O_4Mn$ (301.16): C, 47.86; N, 9.30; H, 3.35. Found: C, 47.84; N, 9.68; H, 3.49. IR (micro-spectrum): 3050w, 2843w, 2764w, 1611sh, 1578s, 1537w, 1400m, 1394m, 1353m, 1223w, 1088w, 1010w, 828m, 776m.

$Co(HCOO)_2$(4,4′-bpy) (2·Co). The synthesis of **2·Co** was similar to that of **1·Mn**. Evaporation of the mother liquid containing $Co(HCOO)_2{\cdot}2H_2O$ and 4,4′-bpy in the molar ratio 1:1 in about 10 days gave red block crystals of **2·Co**. The yield of **2·Co** is about 60%. Anal. (%) Calcd for $C_{12}H_{10}N_2O_4Co$ (305.15): C, 47.23; N, 9.18; H, 3.30. Found: C, 47.23; N, 9.18; H, 3.30. IR (micro-spectrum): 3057w, 2863w, 2769w, 1610sh, 1571s, 1537w, 1489w, 1398dm, 1391dm, 1350m, 1223w, 1091w, 1014w, 832m, 781m.

$Co(HCOO)_2$(4,4′-bpy)·5H_2O (3·Co) and $Ni(HCOO)_2$(4,4′-bpy)·5H_2O (4·Ni). These two compounds were synthesized by the hydrothermal method. $Co(HCOO){\cdot}2H_2O$ or $Ni(HCOO)_2{\cdot}2H_2O$ (0.5 mmol) and 4,4′-bpy (0.5 mmol) in 15 mL of H_2O were heated in a Teflon-lined autoclave (20 mL) at 150 °C for 3 days. After being slow cooled to room temperature, some red/pale blue precipitation was removed from the solution through filtering. Prism crystals (pale pink for **3·Co**, blue for **4·Ni**) suitable for single-crystal X-ray crystallographic analysis were obtained by evaporating the residual solution at room temperature for about 1 week. The crystals were filtered from the mother liquid and washed with ethanol. The yield is about 50%. For **3·Co**, Anal. (%) Calcd for $C_{12}H_{20}N_2O_9Co$ (395.23): C, 36.43; H, 5.10; N, 7.09. Found: C, 37.1; H, 4.99; N, 7.16. IR (micro-spectrum): 3269br, 2880w, 1608s, 1538w, 1493w, 1415w, 1392m, 1365m, 1338w, 1224w, 1071w, 1008w, 825m. For **4·Ni**, Anal. (%) Calcd for $C_{12}H_{20}N_2O_9Ni$ (395.01): C, 36.49; H, 5.10; N, 7.09. Found: C, 36.65; H, 5.30; N, 7.05. IR (micro-spectrum): 3259b, 2888w, 1610d, 1589d, 1539w, 1494w, 1415w, 1393m, 1366m, 1342m, 1224w, 1072w, 1010w, 827m.

Single-Crystal X-ray Crystallography. The data collections of all compounds were made on a NONIUS Kappa-CCD with Mo Kα radiation ($\lambda = 0.71073$ Å) at 293 K. The structures were solved by direct methods and refined by a full matrix least squares technique based on F^2 using the SHELXL 97 program. The hydrogen atoms of 4,4′-bpy and $HCOO^-$ were added to calculated positions. The hydrogen atoms of water in **3·Co** were not added, and those of **4·Ni** were added to calculated positions and fixed. The details of the crystallographic data are listed in Table 1.

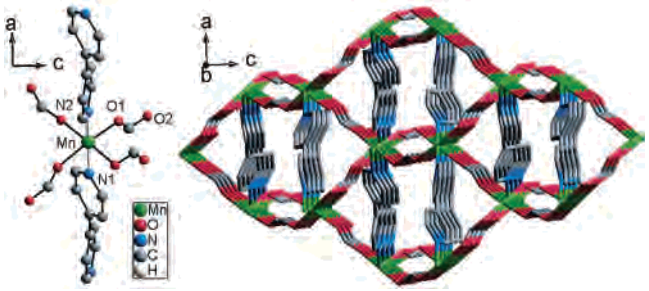

Figure 1. The coordination environment of M ion and the 3D diamondoid structure of **1·Mn** and **2·Co.** Hydrogen atoms were omitted for clarity.

CCDC-239780-239783 contains the supplementary crystallographic data for this paper. These data can be obtained free of charge at www.ccdc.cam.ac.uk/conts/retrieving.html [or from the Cambridge Crystallographic Data Centre, 12, Union Road, Cambridge CB2 1EZ, UK; fax, (internat.) +44-1223/336-033; e-mail, deposit@ccdc.cam.ac.uk]. Also, CIF files of these four compounds can be found in the Supporting Information.

Results and Discussion

Crystal Structures. Details of the crystallography can be found in the Experimental Section. Single-crystal X-ray investigation of **1·Mn** and **2·Co** at 293 K reveals that both of them are isomorphous with the reported $Cu(HCOO)_2(4,4'\text{-bpy})$[9b] with slight differences in the crystal parameters. They are crystallized in the chiral space group $P4_12_12$ as a three-dimensional "diamond" topology if concerning $HCOO^-$ only (Figure 1). Their structures are very similar to that of $Mn(N_3)_2(4,4'\text{-bpy})$ except for the chirality of the lattices (for $Mn(N_3)_2(4,4'\text{-bpy})$, the space group is $P4_32_12$).[14] It will be shown below in the Magnetic Properties section that these two isostructural compounds have similar magnetic properties. The absence of the symmetrical center between the adjacent metal ions bridged by μ-$HCOO^-$ and N_3^- favors the Dzyaloshinsky—Moriya (D—M) interaction, and thus possibly influences the magnetic properties.[15] In both compounds **1·Mn** and **2·Co**, M^{2+} cations are octahedrally coordinated to four O-atoms from four *anti—anti* formates and two N-atoms from two trans-coordinated 4,4′-bpy ligands, and the octahedron is slightly distorted. Their structures are quite complex because all formate ions and 4,4′-bpy act as bridges. As mentioned by S. Martín et al.,[14b] the cages of these two compounds are adamantine-type cages concerning 4,4′-bpy. The 4,4′-bpy ligands are twisted about the C—C bond by 43.6° for Mn and 45.1° for Co, greater than that in $Mn(N_3)_2(4,4'\text{-bpy})$ (31.9°). As in $Mn(N_3)_2(4,4'\text{-bpy})$ and $Cu(HCOO)_2(4,4'\text{-bpy})$, the $M—N_{bpy}$ distances are inequivalent too [2.224 and 2.236 Å for Mn, 2.120 and 2.124 Å for Co]. The intra-network M—M separations are 6.03/5.93 Å (via $HCOO^-$) and 11.52/11.29 Å (via 4,4′-bpy) for Mn and Co, respectively, longer than that of Cu—Cu. The shorter M—M distances in **2·Co** are due to the small radius of Co^{2+} as compared to Mn^{2+}. The longer Cu—Cu distance of 6.07 Å in $Cu(HCOO)_2(4,4'\text{-bpy})$ may arise from the Jahn—Teller distortion which elongates one of the Cu—O bonds up to 2.528 Å (the longest bonds for Mn—O and Co—O are 2.217 and 2.153 Å, respectively), and this distortion of the coordination polyhedra of Cu^{2+} ions influences its magnetic property greatly.[9b]

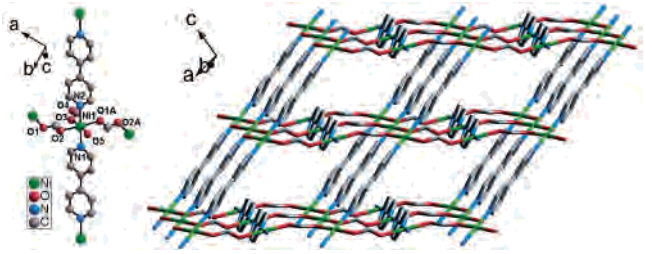

Figure 2. The coordination environment of M ion and the noninterpenetrated "$CdSO_4$" type structure of **3·Co** and **4·Ni**. Hydrogen atoms, the coordination water O5, and the terminal formate O3—C—O4 were omitted for clarity.

Compounds **3·Co** and **4·Ni** are isomorphs in a noncentrosymmetric space group *Cc* with a novel noninterpenetrated $CdSO_4$ type framework. Each metal ion is octahedrally bonded by two bridging 4,4′-bpy, two bridging $HCOO^-$ (O1—C—O2) groups of *anti—anti* mode, all in trans positions around the metal ion, one terminal $HCOO^-$ (O3—C—O4), and one H_2O (Figure 2). The bridging formate ligands link metal ions to form chains running along the *ac* direction. The chain is further connected to other chains via 4,4′-bpy ligands. As the metal ions of one chain are linking other chains along two directions alternatively, the topology of the 3D framework is $CdSO_4$-type. As compared to interpenetrated ones, the noninterpenetrated $CdSO_4$ network was quite rarely observed because of its intrinsically low packing density.[1d,16,17] The framework displays open channels along the *c* direction, which are filled with water molecules. The packing coefficient of the framework is 0.55, and the void space is 27% as calculated by PLATON. The M—N bond distances are 2.157 Å for **3·Co** and 2.103 Å for **4·Ni**, and the averaged M—O distances are 2.12 and 2.08 Å, respectively. The M—M distances bridged by 4,4′-bpy are 11.42 and 11.32 Å and those by formate are 5.93 and 5.89 Å, for **3·Co** and **4·Ni**, respectively. Bpy ligands are slightly twisted. In the metal-formate chain, the coordination polyhedra of neighboring M^{2+} sites have different orientations. Actually, in all compounds **1**—**4**, the axes (N—M—N) of the polyhedron are successively tilted with respected to each other (72.9° for **1** and **2**, 37.6° for **3** and **4** along the formate bridged chain). I. F. Silvera et al. had showed that the anisotropy in the *g* values could give rise to spin-canting if the axes of the *g* tensors are tilted.[18] Also, it has been pointed

(15) (a) Kahn, O. *Molecular Magnetism*; VCH: New York, 1993. (b) Carlin, R. L.; Van-Duyneveldt, A. J. *Magnetic Properties of Transition Metal Compounds*; Springer-Verlag: New York, 1977. (c) Carlin, R. L. *Magnetochemistry*; Springer-Verlag: Berlin Heidelberg, 1986.

(16) (a) Long, D.-L.; Blake, A. J.; Champness, N. R.; Schröder, M. *Chem. Commun.* **2000**, 1369—1370. (b) O'keeffe, M.; Eddaoudi, M.; Li, H.-L.; Reineke, T.; Yaghi, O. M. *J. Solid State Chem.* **2000**, *152*, 3—20. (c) Carlucci, L.; Ciani, G.; Macchi, P.; Proserpio, D. M. *Chem. Commun.* **1998**, 1837—1838. (d) Brooks, N. R.; Blake, A. J.; Champness, N. R.; Cunningham, J. W.; Hubberstey, P.; Teat, S. J.; Wilson, C.; Schröder, M. *J. Chem. Soc., Dalton Trans.* **2001**, 2530—2538.

(17) Carlucci, L.; Gianfranco, Ciani, L.; Proserpio, D. M.; Rizzato, S. *CrystEngComm* **2003**, *5*, 190—199.

(18) Silvera, I. F.; Thornley, J. H. M.; Tinkham, M. *Phys. Rev.* **1964**, *A695*, 136.

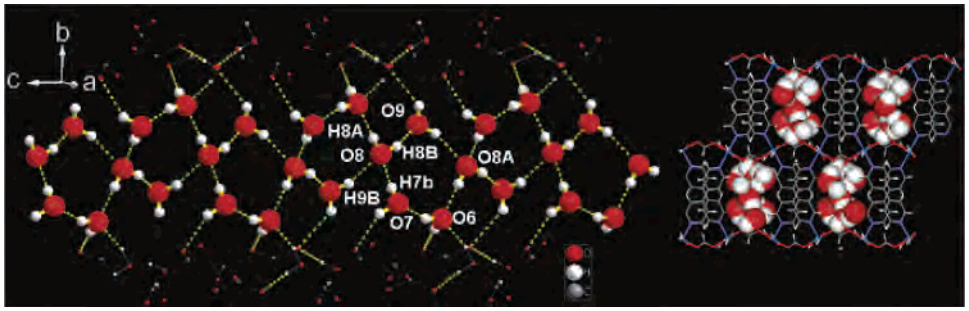

Figure 3. The 1D water T5(1) tape constructed by vertex-sharing cyclic pentamers residing in the channels of **3·Co** and **4·Ni**.

out that this kind of tilting fulfills the symmetry requirement of a lack of an inversion center between the metal ions and thus the moments. This, along with the large anisotropy in the interactions, should be the source of canting for $CsCoCl_3 \cdot 2H_2O$, $[(CH_3)_3NH]CoCl_3 \cdot 2H_2O$, and α-$CoSO_4$.[15b] So, it may have a great influence on the magnetic properties of our four compounds. As a matter of fact, compounds **1**, **2**, and **4** are indeed proved to be spin-canted weak ferromagnets.

The water molecules in the channels (Figure 3) of the framework show interesting characteristics. When forming hydrogen bonds with the oxygens from the formates and the coordinated H_2O of the framework, the water molecules themselves form cyclic water pentamer, and these pentamers further build into a tape by sharing vertex. According to L. Infantes,[19] this water tape is the first example of "T5(1)" ("T" means "tape", "5" represents the number of the waters in an individual ring, "1" means one sharing water). Some examples of "T5" tape have been reported, but they are edge-sharing pentamers (denoted as "T5(2)") or isolated pentamers (denoted as "T5(0)"). The envelope conformation of the pentamers is similar to that of cyclopentane, in agreement with the puckered ring achieved from both experimental and theoretical studies by Liu, Saykally, and co-workers.[20] The distances between the neighboring oxygens in the pentamers are O6−O7 2.75, O7−O8 2.78, O8−O9 2.73, O9−O8a 3.07, and O8A−O6 2.79 Å. The distance of O9−O8a (3.07 Å) is somewhat longer than normal, and the others are fit well to the value (2.73 Å) obtained by DFT.[21] The adjacent pentamers with the sharing vertex are not coplanar but are twisted with each other. This arrangement is reasonable because of the geometry of the vertex oxygen O8. The polyhedron of the O8 formed by hydrogen atoms is a distorted tetrahedron with the bond angels of ∠H−O8−H as follows: ∠H8a−O8−H8b 105°, ∠H8b−O8···H7b 109°, ∠H7b···O8···H9b 77°, and ∠H9b···O8···H8a 116°. All water molecules in the structure can be removed by thermal treatment. The TGA of **3·Co** and **4·Ni** reveals that the loss of water occurs before 90 °C and then the weight keeps constant up to 210 °C following the decomposition of the residues (Figure S1).

Water structures are the focus of the current experimental and theoretical studies due to the importance of water in chemical processes and biological systems.[22] Numerous water clusters[23] and some 1D[24] and 2D[25] water systems consisting of the basic cyclic water ring units have been found in a number of crystal hosts that offer attractive environments for stabilizing water clusters. These trapped waters provide quantitative characterization of their behaviors and hold considerable promise for achieving the more accurate description of the properties of bulk water at a molecular level and new concepts of some biological processes. The tape pattern is very rare (4.6% according to L. Infantes), and no example has been reported of the T5(1) pattern. The first T5(1) water tape in this work offers a good example for understanding well the water structures.

The corresponding azide compounds of Co and Ni formulated as $M(N_3)_2(4,4'\text{-bpy})$[14b] differ greatly from the formates **2**−**4**, arising from the different coordination properties of formate and azide. Actually, the oxygen atom behaves as a harder acid than does nitrogen, which, together with the geometries of azide and formate, influences the formation and structures of the complexes. Obviously, different struc-

(19) Infantes, L.; Motherwell, S. *CrystEngComm* **2002**, *4*, 454−461.
(20) Liu, K.; Brown, M. G.; Cruzan, J. D.; Saykally, R. J. *Science* **1996**, *271*, 62.
(21) (a) Xantheas, S. S.; Dunning, T. H., Jr. *J. Chem. Phys.* **1993**, *99*, 8774. (b) Xantheas, S. S.; Dunning, T. H., Jr. *J. Chem. Phys.* **1993**, *98*, 8073. (c) Xantheas, S. S. *J. Chem. Phys.* **1995**, *102*, 4505.
(22) (a) Liu, K.; Brown, M. G.; Carter, C.; Saykally, R. J.; Gregory, J. K.; Clary, D. C. *Nature* **1996**, *381*, 501. (b) Nauta, K.; Miller, R. E. *Science* **2000**, *287*, 293. (c) Weinhold, F. *J. Chem. Phys.* **1998**, *109*, 367. (d) Ugalde, J. M.; Alkorta, I.; Elguero, J. *Angew. Chem.* **2000**, *112*, 733; *Angew. Chem., Int. Ed.* **2000**, *39*, 717. (e) Ludwig, R. *Angew. Chem.* **2001**, *113*, 1856; *Angew. Chem., Int. Ed.* **2001**, *40*, 1808. (f) Kim, J.; Majumdar, D.; Lee, H. M.; Kim, K. S. *J. Chem. Phys.* **1999**, *110*, 9128. (g) Liu, K.; Cruzan, J. D.; Saykally, R. J. *Science* **1996**, *271*, 929.
(23) (a) Supriya, S.; Manikumari, S.; Raghavaiah, P.; Das, S. K. *New J. Chem.* **2003**, *27*, 218. (b) Doedens, R. J.; Yphannes, E.; Khan, M. I. *Chem. Commun.* **2002**, 62. (c) Moorthy, J. N.; Natarajan, R.; Venugopalan, P. *Angew. Chem.* **2002**, *114*, 3567; *Angew. Chem., Int. Ed.* **2002**, *41*, 3417. (d) Atwood, J. L.; Barbour, L. J.; Ness, T. J.; Raston, C. L.; Raston, P. L. *J. Am. Chem. Soc.* **2001**, *123*, 7192. (e) Blanton, W. B.; Gordon-Wylie, S. W.; Clark, G. R.; Jordan, K. D.; Wood, J. T.; Geiser, U.; Collins, T. J. *J. Am. Chem. Soc.* **1999**, *121*, 3551. (f) Barbour, L. J.; Orr, G. W.; Atwood, J. L. *Nature* **1998**, *393*, 671. (g) Barbour, L. J.; Orr, G. W.; Atwood, J. L. *Chem. Commun.* **2000**, 859.
(24) (a) Pal, S.; Sankaran, N. B.; Samanta, A. *Angew. Chem.* **2003**, *115*, 1783; *Angew. Chem., Int. Ed.* **2003**, *42*, 1741. (b) Custelcean, R.; Afloroaei, C.; Vlassa, M.; Polverejan, M. *Angew. Chem.* **2000**, *112*, 3224; *Angew. Chem., Int. Ed.* **2000**, *39*, 3094.
(25) (a) Park, K. M.; Kuroda, R.; Iwamoto, T. *Angew. Chem.* **1993**, *105*, 939; *Angew. Chem., Int. Ed. Engl.* **1993**, *32*, 884. (b) Raghuraman, K.; Katti, K. K.; Barbour, L. J.; Pillarsetty, N.; Barnes, C. L.; Katti, K. V. *J. Am. Chem. Soc.* **2003**, *125*, 6955. (c) Janiak, C.; Scharman, T. G. *J. Am. Chem. Soc.* **2002**, *124*, 14010. (d) Ma, B.-Q.; Sun, H.-L.; Gao, S. *Angew. Chem.* **2004**, *116*, 1398; *Angew. Chem., Int. Ed.* **2004**, *43*, 1374−1376.

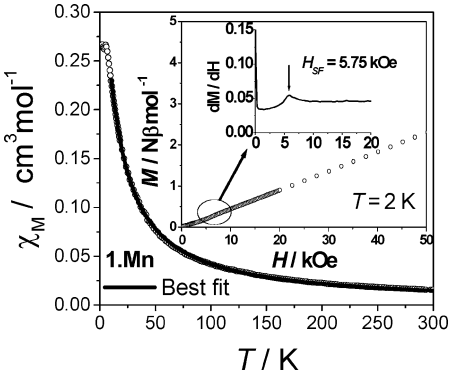

Figure 4. Temperature dependence of χ_M of **1·Mn** at $H = 10$ kOe from 2 to 300 K. Points are experimental data; the line is the best-fit using the model mentioned in the text. Inset: field-dependent isothermal magnetization $M(T,H)$ for **1·Mn** at 2 K and the dM/dH curve, indicating the spin-flop transition.

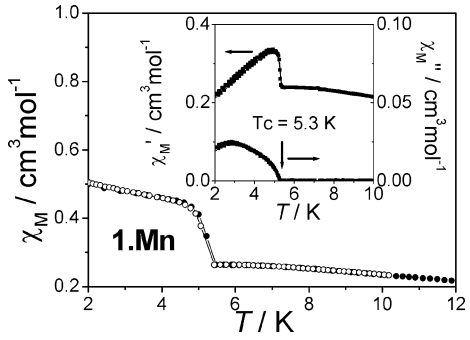

Figure 5. ZFCM and FCM of **1·Mn** at an external field of 200 Oe. Insert: ac magnetic susceptibilities in zero applied dc field and an ac field of 2 Oe at different frequencies (277, 666, 1633, 4111 Hz) for **1·Mn**.

tures will lead to different magnetic properties, as will be shown below.

Magnetic Properties. 1·Mn. Temperature dependence of the magnetic susceptibility χ_M of **1·Mn** in a magnetic field of 10 kOe from 2 to 300 K shows a peak at 5.4 K (Figure 4). The $\chi_M T$ value at 300 K is 4.57 cm^3 K mol^{-1} and decreases upon cooling to 0.64 cm^3 K mol^{-1} at 2.4 K. The magnetic susceptibility data in the range of 20−300 K obey the Curie−Weiss law, $\chi_M = C/(T - \theta)$, with a Curie constant $C = 4.72$ cm^3 K mol^{-1}, which is slightly larger than the spin-only value of 4.375 cm^3 K mol^{-1} for a Mn^{2+} ion, and a negative Weiss constant θ of −11.3 K, which indicates the antiferromagnetic interaction between Mn^{2+} ions (Figure S2). Both the temperature dependence of the zero-field-cooled and the temperature dependence of the field-cooled magnetization (ZFCM and FCM) measured in a low field of 200 Oe show abrupt increases at ca. 5.2 K (Figure 5). This behavior may arise from the onset of long-range ordering. Ac magnetic susceptibility with frequencies of 277, 666, 1633, and 4111 Hz was measured under $H_{dc} = 0$ Oe and $H_{ac} = 2$ Oe from 2 to 10 K (inset of Figure 5). Both the in-phase and the out-of-phase signals show an abrupt increase at ca. 5.3 K, and no frequency dependence was observed. The occurrence of the nonzero out-of-phase signal indicates that there exists a spontaneous magnetization below 5.3 K and the temperature is very close to the peak temperature of d(χ_M)/dT (5.2 K) (Figure S3).

To clarify the nature of the low-temperature phase, we have measured the isothermal magnetization $M(T,H)$ at 2 K with field up to 50 kOe (inset of Figure 4). The magnetization increases almost linearly at field range 0−5 kOe, and after an abnormality at about 5−6 kOe, it increases up to 50 kOe and reaches 2.31 μ_B per Mn^{2+}, far from the saturation value $M_S = 5\ \mu_B$ for a spin-only Mn^{2+} ion. The $M(T,H)$ behavior is typical for an antiferromagnet, and the slight abnormality of magnetization at 5−6 kOe indicates that a spin-flop transition occurs, as can be found in many antiferromagnets with weak anisotropy (e.g., Mn^{2+}).[15b,c] The critical field $H_{SF} = 5.75$ kOe, which is the peak in the curve of dM/dH. Careful examination in the low-field region revealed that no detected hysteresis loop was observed at 1.8 K but the remnant magnetization M_R is 0.007 μ_B, arising from the spontaneous magnetization (Figure S4). Based on those results of ZFCM/FCM, ac susceptibility, and isothermal magnetization, **1·Mn** is a 3D weak ferromagnet due to spin-canting with the critical temperature $T_c = 5.3$ K. The canting angle α is related to M_R and M_S through $\sin(\alpha) = M_R/M_S$[15a] and is estimated to be about 0.08°.

On the basis of the structure, the high-temperature χ_M of **1·Mn** may be analyzed by the HTS model deduced from the results developed by Rushbrook and Wood[26] for a Heisenberg antiferromagnet ($S = {}^5/_2$) for a diamond-type network (say, $z = 4$ and $p_4 = 6$, see ref 26) with the Hamiltonian $H = -2J\sum_{\langle i,j\rangle} S_i \cdot S_j$,

$$\chi = \frac{Ng^2\beta^2 S(S+1)}{3k_B T}(1 + \sum_{n=1}^{6} C_n x^n)^{-1} \qquad (1)$$

with $x = J/k_B T$, and $C_1 = -23.3333$, $C_2 = 147.778$, $C_3 = -405.487$, $C_4 = -1621.13$, $C_5 = 14\,201$, and $C_6 = 1\,037\,840$. N, J, g, β, S, k_B, and T have their usual meanings. The best fitting of the data above 10 K (see Figure 4) gives $J = -0.23$ cm$^{-1} = -0.33$ K, $g = 2.03$ with $R = 8.3 \times 10^{-5}$ [$R = [\sum(\chi_{obs} - \chi_{calc})^2/\sum(\chi_{obs})^2]$], which shows quite well the experiment−theory agreement and is consistent with that reported for Mn−O−C(R)−O−Mn interactions (−0.2 to −0.3 cm^{-1}).[10a] At the same time, according to the molecular-field theory of antiferromagnetism,[15]

$$T_C = 2S(S+1)zJ/3k_B \qquad (2)$$

where z is the magnetic coordination number of a lattice site. For **1·Mn**, $T_c = 5.3$ K, $S = {}^5/_2$, and $z = 4$, we get $J = 0.15$ cm$^{-1} = 0.22$ K, as is comparable to that deduced from eq 1.

The structural similarity of $Mn(N_3)_2$(4,4′-bpy)[14] and **1·Mn** provides the chance to compare their magnetic properties and offers us a glance of the similarity and the difference of azide and formate. Similar to **1·Mn**, $Mn(N_3)_2$(4,4′-bpy) behaves as a weak ferromagnet also due to spin-canting. It shows us that both azide and formate in 2.11 mode can mediate antiferromagnetic interactions, as reported in numerous reports. The main difference between them is the magnitude of the magnetic interactions mediated by azide

(26) Rushbrook, G. S.; Wood, P. *J. Mol. Phys.* **1958**, *1*, 257−283.

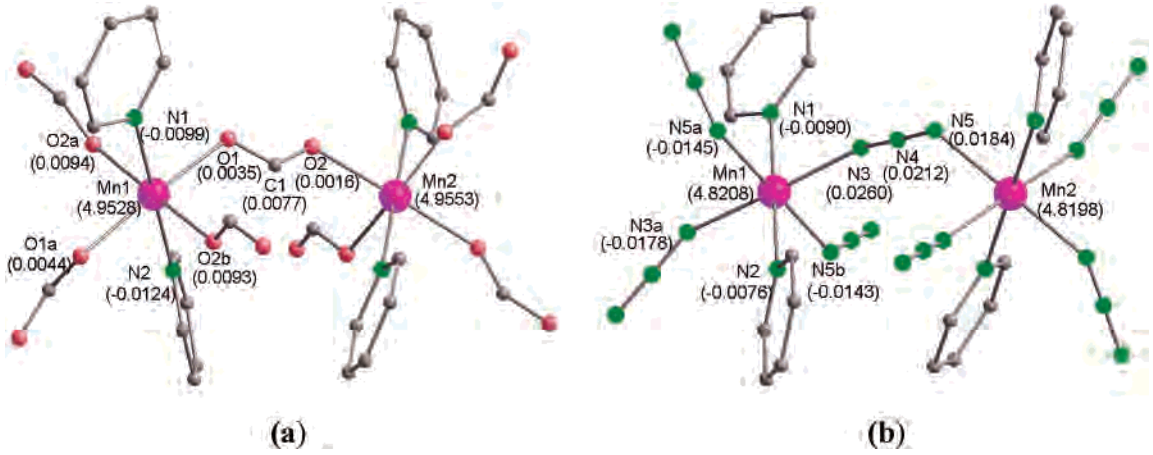

Figure 6. Model compounds based on the actual molecular structures for DFT calculation. The numbers in the parentheses are the calculated spin populations on the selected atoms. (a) $[Mn_2(HCOO)_6(\mu\text{-}HCOO)(py)_4]^{3-}$, (b) $[Mn_2(\mathbf{N_3})_6(\mu\text{-}1,3\text{-}N_3)(py)_4]^{3-}$.

Table 2. Some Selected Magnetic Parameters for Two Classes of Metal Formates and Metal Azides

		T_c/K	Weiss constant θ/K	J/cm^{-1}	α/deg	ref
I	1·Mn	5.3	−11.3	−0.19	0.08	this work
	$Mn(N_3)_2$(4,4-bpy)	42.5	−100	−1.92	0.5	14
II	$Mn(HCOO)_3[NH_2(CH_3)_2]$	8.5	−16.3	−0.23	0.08	13a
	$Mn(N_3)_3[N(CH_3)_4]$	∼70		−1.73		13c,d

and formate. Some magnetic parameters are listed in Table 2. For **1·Mn**, the critical temperature T_c, the Weiss constant θ, the exchange value J fitted by the same model, and the estimated canting angle α are all smaller than those of $Mn(N_3)_2$(4,4′-bpy). It is obvious that μ-1,3-N_3^- mediates stronger antiferromagnetic interaction between spin carriers than does *anti*−*anti* $HCOO^-$. A similar conclusion can also be drawn from the comparison of the other paired similar compounds $Mn(HCOO)_3[NH_2(CH_3)_2]$[13a,b] and $Mn(N_3)_3[N(CH_3)_4]$,[13c,d] both of NaCl type frameworks. The critical temperature and the J value are all higher in the azide compound.

To arrive at a better understanding of the similarity and difference of the magnetic coupling interaction between Mn−Mn through the bridging ligands $HCOO^-$ and N_3^- theoretically, quantum chemical density functional theory (DFT) calculations, by using the Amsterdam Density Functional (ADF) package version 2004.01[27] combined with the broken symmetry approach (DFT-BS),[28] were performed. Herein, our emphasis will be lie on the nature of the magnetic coupling interaction between the paramagnetic ions. Thus, for the three-dimensional diamond-like structure **1·Mn** and its azide analogue,[14] for simplicity, we calculated only the model compounds of the dimer units, $[Mn_2(HCOO)_6(\mu\text{-}1,3\text{-}HCOO)(py)_4]^{3-}$ and $[Mn_2(N_3)_6(\mu\text{-}1,3\text{-}N_3)(py)_4]^{3-}$ (py = pyridine) (Figure 6), where the mono-bridge ligand mediates the two paramagnetic ions Mn1 and Mn2. In the calculations, the geometrical configurations of the model complexes adapted the experimental crystal structure data. The details of the calculation method were described elsewhere.[29]

On the basis of DFT-BS calculations, the relative magnitude of the magnetic coupling interactions for these two model compounds was reproduced. The calculated magnetic coupling constants J for the $HCOO^-$ and N_3^- bridged model compounds are −0.58 and −5.21 cm^{-1}, as compared to the experimental fitting J values of −0.19 and −1.92 cm^{-1}, respectively. Both the calculated and the experimental J values indicate consistently that the weak antiferromagnetic coupling between Mn1 and Mn2 occurs through $HCOO^-$ and N_3^- bridging ligands, and μ-1,3-N_3^- mediates the stronger antiferromagnetic coupling than that for *anti*−*anti* $HCOO^-$.

The spin density distribution in the magnetic systems has been proposed to obtain some valuable hints for the magnetic coupling interaction. Some coupling mechanisms have been proposed to explain the magnetic coupling behavior between two metal centers. Among them, the spin delocalization[15a] and spin polarization mechanisms[30] succeed in dealing with the mononuclear and homobinuclear systems.[31] From the point of view of molecular orbital theory, the spin delocalization can be explained as a transfer of unpaired electron density from the metal atom to the ligand atoms, while the spin polarization results from the optimization of the electronic exchange and Coulomb terms and induces the spin distribution with alternating sign for the successive ligand atoms.

On the basis of the Mulliken population analysis, we calculated the spin populations on the selected atoms in the high-spin state, given by numbers in parentheses in Figure 6, where the plus and minus signs indicate α and β spin

(27) Amsterdam Density Functional (ADF), version 2004.01; Scientific Computing and Modelling, Theoretical Chemistry, Vrije Universiteit, Amsterdam, 2004.
(28) (a) Noodleman, L. *J. Chem. Phys.* **1981**, *74*, 5737. (b) Noodleman, L.; Baerends, E. J. *J. Am. Chem. Soc.* **1984**, *106*, 2316.
(29) (a) Yan, F.; Chen, Z.-D. *J. Phys. Chem. A* **2000**, *104*, 6295. (b) Ren, Q.-H.; Ren, J.; Wei, H.-Y.; Wang, F.; Zhang, L.; Chen, Z.-D. *J. Phys. Chem. A* **2002**, *106*, 6161.
(30) (a) McConnell, H. M. *J. Chem. Phys.* **1963**, *39*, 1910. (b) Izuoka, A.; Murata, S.; Sugawara, T.; Iwamura, H. *J. Am. Chem. Soc.* **1987**, *109*, 2631. (c) Charlot, M.-F.; Kahn, O.; Chaillet, M.; Larrieu, C. *J. Am. Chem. Soc.* **1986**, *108*, 2574. (d) Albright, T. A.; Burdett, J. K.; Whangbo, M.-H. *Orbital Interactions in Chemistry*; Wiley: New York, 1985.
(31) Cano, J.; Ruiz, E.; Alvarez, S.; Verdaguer, M. *Comments Inorg. Chem.* **1998**, *20*, 27.

states, respectively. It is found that for the two model compounds the spin populations on paramagnetic Mn ions have the same sign as that on the atoms of the bridging ligand. It is indicated that the same spin delocalization mechanism occurs in both the N_3^- and the $HCOO^-$ bridged model compounds. On the other hand, the spin population on the Mn1 atom is 4.8208 for the N_3^- bridged model, smaller than 4.9528 of the $HCOO^-$ bridged model. It is evident that the spin delocalization from the Mn magnetic center to bridging N_3^- is stronger than that to $HCOO^-$, while the bridging N_3^- ligand, N3 (0.0260), N4 (0.0212), and N5 (0.0184), has larger spin population than the bridging ligand $HCOO^-$, O1 (0.0035), C1 (0.0077), and O2 (0.0016). Thus, N_3^- mediates a stronger exchange coupling.

Magnetic orbital analysis is often used to explore the pathway of magnetic coupling in magnetic molecules. From the single determinant calculation in ADF, the single occupied molecular orbitals in the high-spin state can be obtained. These orbitals are termed as molecular magnetic orbitals, which are composed of the local magnetic orbitals located on each paramagnetic center, respectively. On the other hand, on the basis of the calculation on the antiferromagnetic configuration by using the broken symmetry approach, we can also obtain the local magnetic orbitals,[32] which describe the distribution of the active spin electrons on each local magnetic center. Besides the paramagnetic metal ion, in general, these local magnetic orbitals contain possible components of bridging and/or terminal ligands. It is beyond any doubt that the analysis for these local magnetic orbitals is an enlightening discussion to understand the similarities and the differences of the magnetic coupling interaction between Mn−Mn through the bridging ligands $HCOO^-$ and N_3^-, respectively.

For the convenience of orbital analysis, in the site coordination of the molecular fragment containing Mn1, the Mn−N1 was taken as the apical direction, and the metal orbital $d_{x^2-y^2}$ as the *xy* plane, pointing toward the four O-atoms from four *anti−anti* formats. Figure 7 shows the calculated local magnetic orbitals for the model compounds studied by using the broken symmetry approach. It is shown in Figure 7 that in these local magnetic orbitals, beside the d-orbitals on the Mn1 ion, the bridging ligand also participates in the constitution of the local magnetic orbital and reveals the coupling pathway. It is evident that, differing from the formate or azide ion bridged copper analogues, there are five d orbitals in the high-spin Mn(II) ion involved in the magnetic coupling. In the former, only the $d_{x^2-y^2}$ orbital in the Cu(II) ion participates in magnetic coupling in σ fashion with the bridging ligand,[33] while in the **1·Mn** and $Mn(N_3)_2$-(4,4′-bpy) the coupling interaction of the Mn(II) ions through the bridging ligand occurs in both σ ($d_{x^2-y^2}$, d_{z^2}) and π (d_{xz}, d_{yz}) fashions. From these local magnetic orbitals, the molecular magnetic orbitals can be constructed through their combination. In further inspection of the overlap integral

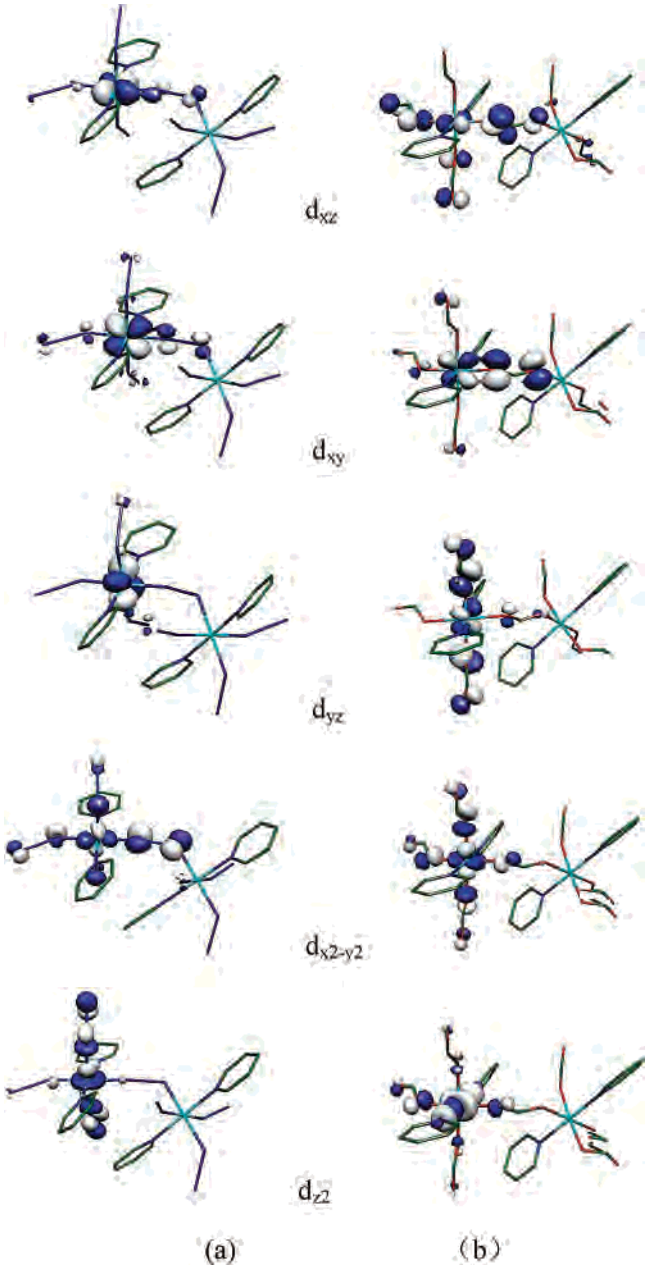

Figure 7. Local magnetic orbitals for the model compounds (a) Mn−N_3^-, and (b) Mn−$HCOO^-$.

between these local magnetic orbitals, it is found that except for the larger overlap of π-type from d_{xy} and d_{xz} orbitals, the azide ion bridged model compound reveals the stronger σ-overlap from the $d_{x^2-y^2}$ orbital. For the azide ion bridged model compound, the overlap integral (0.5477) between local magnetic orbitals on Mn1 and Mn2 ions is larger than in the formate ion bridged model compound (0.3018) (cf., Table 3). The larger overlap between the local magnetic orbitals represents the stronger antiferromagnetic coupling interaction between the paramagnetic ions. Thus, N_3^- mediates a stronger exchange coupling. It is evident that both spin population and magnetic orbitals analyses reveal the similarities and the differences of the magnetic coupling interaction in the formate and azide bridged analogues.

Because of the difference in the electronic nature of the oxygen and nitrogen atoms, the coordination abilities of azide

(32) Liu, C.; Hu, H.; Yang, X. *Chem. Phys. Lett.* **2001**, *349*, 89.
(33) Comarmond, J.; Plumere, P.; Lehn, J.-M.; Agnus, Y.; Louis, R.; Weiss, R.; Kahn, O.; Morgenstern-Badarau, I. *J. Am. Chem. Soc.* **1982**, *104*, 6330.

Table 3. Overlap Integral among Local Magnetic Orbitals ϕ_i^A and ϕ_j^B Involved in Magnetic Coupling[a]

	$\sum_j \phi_j^B/\phi_i^A$					
	d_{z^2}	$d_{x^2-y^2}$	d_{yz}	d_{xy}	d_{xz}	$\sum S_{ij}^{AB}$
Mn−HCOO$^-$	0.0020	0.0037	0.0151	0.1413	0.1397	0.3018
Mn−N$_3^-$	0.0071	0.1752	0.0021	0.2822	0.0811	0.5477

[a] ϕ_i^A and ϕ_j^B denote the local magnetic orbital on A molecular fragment and B molecular fragment, respectively. The data in the last column are a sum over all *i* and *j* for ϕ_i^A on A and ϕ_j^B on B, respectively, and other data in the table are the sum over all *j* for ϕ_j^B on B.

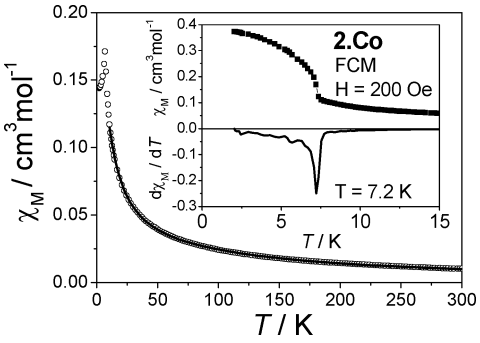

Figure 8. Temperature dependence of χ_M of **2·Co** at $H = 10$ kOe from 2 to 300 K. Inset: FCM of **2·Co** at an external field of 200 Oe and the differentiate of FCM.

and formate are not the same, and it may sometimes lead to different structures and hence magnetic properties. As can be seen below, **2·Co**, **3·Co**, and **4·Ni** are the proper examples showing these differences.

2·Co. The overall magnetic property of **2·Co** is quite similar to that of **1·Mn** as isostructures. The temperature dependence of the magnetic susceptibility χ_M of **2·Co** from 2 to 300 K shows a sharp peak at 6.8 K (Figure 8), which suggests the presence of an antiferromagnetic ordering. The $\chi_M T$ value at 300 K is 3.00 cm^3 K mol^{-1}, which is significantly larger than the spin-only value 1.875 cm^3 K mol^{-1} and decreases upon cooling to 0.32 cm^3 K mol^{-1} at 2.2 K. Fitting the χ_M data in 10−300 K with the Curie−Weiss law gives a Curie constant $C = 3.41$ cm^3 K mol^{-1} and Weiss constant $\theta = -40.2$ K (Figure S2). The high value of C (1.875 cm^3 K mol^{-1} for spin-only Co^{2+}) and the big negative θ may be partly contributed by the strong spin−orbit coupling, which is remarkable for the $^4T_{1g}$ state of Co^{2+} in an octahedral ligand field. From the fitted Curie constant C, one can deduce the g value to be about 2.70. The not small negative θ may also indicate the antiferromagnetic coupling between adjacent Co^{2+} ions, which is found in other cobalt complexes bridged by *anti*−*anti* HCOO$^-$.

For high-spin octahedral Co^{2+} (d^7, $S = 3/2$), the ground state $^4T_{1g}$ is always difficult to magnetically analyze because of the unquenched spin−orbit coupling in the ligand environment with high symmetry as well as zero-field splitting effects. Although difficult, some efforts have been made to calculate the spin−orbit coupling parameter λ ($\lambda = -170$ cm^{-1} for free ion), the axial splitting parameter Δ (and then the axial zero-field splitting parameter D), and/or the exchange coupling parameter J for some mono- and binuclear Co^{2+} in octahedral field.[34−36] In particular, the Magsaki software developed by H. Sakiyama can effectively calculate the magnetic susceptibility and effective magnetic moment for mono- and dinuclear Co^{2+} in the isotropic or axially distorted octahedral field and gives λ, Δ, g, and J.[36] In the case of **2·Co**, we treat the susceptibility data by considering a mononuclear Co^{2+} with spin−orbit coupling parameter λ ($H = -\lambda LS$) in a molecular-field approximation. The χ_{mono} for a mononuclear Co^{2+} in an octahedral environment can be calculated from eq 3,[34]

$$\chi_{mono} = \frac{1}{T}*\left[\frac{7(3-A)^2x}{5} + \frac{12(2+A)^2}{25A} + \left\{\frac{2(11-2A)^2x}{45} + \frac{176(2+A)^2}{675A}\right\}x\exp\left(\frac{-5Ax}{2}\right) + \left\{\frac{(5+A)^2x}{9} - \frac{20(2+A)^2}{27A}\right\}\exp(-4Ax)\right] \Big/ \left[\frac{8x}{3}\left\{3 + 2\exp\left(\frac{-5Ax}{2}\right) + \exp(-4Ax)\right\}\right] \quad (3)$$

with $x = \lambda/k_BT$. The parameter A gives a measure of the crystal field strength relative to the interelectronic repulsions and is equal to 1.5 for a weak crystal field, 1.32 for a free ion, and 1.0 for a strong field. Considering the molecular-field theory with zJ as the total exchange parameter between Co^{2+} ions, we can fit our experiment data with eq 4,[15]

$$\chi = \frac{\chi_{mono}}{1 - (2zJ/Ng^2\beta^2)\chi_{mono}} \quad (4)$$

In eqs 3 and 4, N, g, β, k_B, and T have their usual meanings. The best fitting of the susceptibility data in the temperature range 10−300 K gives $\lambda = -147$ cm^{-1} $= -213$ K, $A = 1.25$, and z$J = -1.37$ cm^{-1} $= -1.98$ K with $R = 7.4 \times 10^{-5}$ [$R = [\sum(\chi_{obs} - \chi_{calc})^2/\sum(\chi_{obs})^2]$. Taking into account that $\lambda = k\lambda_{freeion}$,[34] where k is a reduction of the spin−orbit coupling due to covalency, k is 0.86. The negative value of zJ indicates that the magnetic coupling between Co^{2+} ions is antiferromagnetic, which is mediated dominantly by *anti*−*anti* 2.11-HCOO$^-$. In view of the diamond topology of **2·Co**, the number of the nearest neighbor of one Co^{2+}, say z, is 4. So one can deduce the antiferromagnetic coupling J to be -0.34 cm^{-1}. Of course, because of the impreciseness of the molecular-field theory, the results we got are approximate and half-quantitative. EPR (electronic paramagnetic resonance) and anisotropic magnetic measurements performed on fine big single crystals are needed for further investigations.

To further clarify the nature of the low-temperature phase, we have measured the FCM in 200 Oe (inset of Figure 8) and the ac magnetic susceptibility under $H_{dc} = 0$ Oe and $H_{ac} = 2$ Oe with frequencies of 277, 666, 1633, and 4111 Hz from 2 to 15 K (Figure S5). The FCM increases abruptly, and the in-phase signal of ac shows a sharp peak at ca. 7.4

(34) Mabbs, F. E.; Machin, D. J. *Magnetism and Transition Metal Complexes*; Chapman and Hall: London, 1973.
(35) Figgis, B. N.; Gerloch, M.; Lewis, J.; Mabbs, F. E.; Webb, G. A. *J. Chem. Soc. A* **1968**, 2086−2093 and references therein.
(36) Sakiyama, H. *J. Chem. Software* **2001**, *7*, 171−178 and references therein.

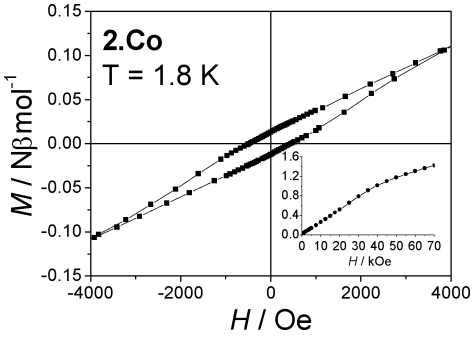

Figure 9. Hysteresis loop for **2·Co** at 1.8 K. Inset: isothermal magnetization $M(T,H)$ at 1.8 K from 0 to 70 kOe.

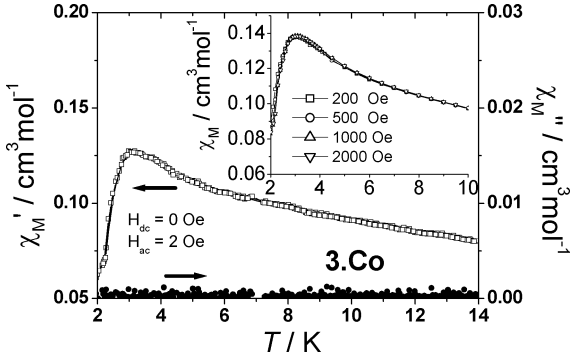

Figure 10. The ac susceptibilities in zero applied dc field and an ac field of 2 Oe at different frequencies (277, 666, 1633, 4111 Hz) for **3·Co**. Inset: FCM of **3·Co** in external fields of 200, 500, 1000, and 2000 Oe.

K, close to that of 7.2 K for the peak of $d(\chi_M)/dT$ (inset of Figure 8). No detectable out-of-phase signal χ''_M and frequency dependence was observed. The absence of the χ''_M component suggests that **2·Co** may be a hidden spin-canted weak ferromagnet, as is characteristic of a system with hidden canting.[15c,37]

The isothermal magnetization $M(T,H)$ at 1.8 K with field up to 70 kOe and the hysteresis loop at 1.8 K have been shown in Figure 9. The spontaneous magnetization at zero field is about 0.013 μ_B. The magnetization increases almost linearly with field up to 40 kOe, and then increases with a smaller slope up to 1.43 μ_B per Co^{2+} at 70 kOe, far from the expected saturation value for one Co^{2+} ion. This behavior strongly suggests the antiferromagnetic coupling between Co^{2+} ions. At 1.8 K, a hysteresis loop can be observed with the coercivity field H_C about 460 Oe and the remnant magnetization $M_R = 0.013\ \mu_B$. All of these results suggest that **2·Co** is a canted weak ferromagnet below 7.4 K. The canting angle α is estimated to be about 0.3°.

The magnetic properties of **1·Mn** and **2·Co** are similar, as they all are weak ferromagnets, but different from that of the isomorphous compound $Cu(HCOO)_2$(4,4′-bpy). We think that the distinct nature of the metallic cation must play an important role in the magnetism. As discussed by J. L. Manson,[9b] $Cu(HCOO)_2$(4,4′-bpy) exhibits 1D ferromagnetism at low temperatures. With a simplified calculation by considering the Cu^{2+} dimers bridged by formate or 4,4′-bpy, they claimed that the antiferromagnetic coupling transmitted by formate may be negligibly small in this compound so the net spin exchange is ferromagnetic. Furthermore, they suggested that a structural phase transition, such as a switch of the Jahn—Teller axis, might change the magnetic orbital from the CuO_2N_2 to the CuO_4 square and disable the antiferromagnetic interaction via 4,4′-bpy.

3·Co. The temperature dependence of χ_M of **3·Co** measured in 1 kOe from 2 to 300 K shows a sharp peak at 3.0 K (Figure S7). The $\chi_M T$ value at room temperature is ca. 3.12 $cm^3\ K\ mol^{-1}$ and decreases smoothly with the decreasing temperature. Fitting χ_M data in the range 10—300 K with the Curie—Weiss law gives a Curie constant $C = 3.36\ cm^3\ K\ mol^{-1}$ and a negative Weiss constant $\theta = -22.7$ K (Figure S6). The high value of C (for spin-only Co^{2+}, $C = 1.875\ cm^3\ K\ mol^{-1}$) and also the negative θ may be partly contributed by the strong spin—orbit coupling. As **2·Co**, a g value is calculated to be 2.68 based on the Curie constant C. Similar to **2·Co**, we treat the magnetic data with eqs 3 and 4. The best fitting of the magnetic susceptibility above 30 K gives $\lambda = -110\ cm^{-1} = -159$ K, $A = 1.30$, and $zJ = -1.67\ cm^{-1} = -2.42$ K with $R = 1.2 \times 10^{-5}$ [$R = [\sum(\chi_{obs} - \chi_{calc})^2/\sum(\chi_{obs})^2]$. The relative smaller value of λ as compared to **2·Co** suggests a larger reduction of the spin—orbit coupling; this might be due to the larger distortion of the coordination octahedron of Co^{2+} in **3·Co**.

Both FCM in 200 Oe and the in-phase ac susceptibility χ'_M under $H_{dc} = 0$ Oe and $H_{ac} = 2$ Oe show peaks at ca. 3.0 K (Figure 10), suggesting a phase transition to an antiferromagnetic ordered state. No resolving out-of-phase signal and frequency dependence (selected frequencies are 277, 666, 1633, and 4111 Hz) were observed. The field dependence of magnetization at 1.8 K shows two abrupt changes at ca. 3 and 9 kOe and keeps on increasing linearly up to 70 kOe (inset of Figure S7). The value of M per Co^{2+} at 70 kOe, ca. 1.45 μ_B, is far from the saturated value for Co^{2+}, which strongly indicates the dominating antiferromagnetic coupling between Co^{2+} ions. No hysteresis loop was observed at 1.8 K. The two transitions of M versus H were further confirmed by the ac isothermal magnetization measurement with the dc field from 0 to 70 kOe and the frequency 666 Hz. Two sharp peaks of χ'_M and the nonzero χ''_M are consistent with the peaks of dM/dH (Figure S8).

To further investigate the low-temperature magnetic behavior of **3·Co**, we have measured the isothermal magnetization at different temperatures (from 1.8 to 3 K with the step 0.2 K) and the susceptibility from 2 to 10 K in different fields (200, 500, 1000, and 2000 Oe). These results are presented in the insets of Figures 10 and 11. At low temperatures ≤ 2.4 K, the magnetization curves show two obvious transitions, and the dM/dH curves (inset of Figure 11) also show two separated peaks, although the exact values for the peaks are changed regularly: the H values for the first peaks increase with the temperature, while it is inverse for the second peaks. On increasing the temperature, the two-step transition disappears and those two peaks become one in dM/dH. As for the susceptibility measurements in different fields from 200 to 2000 Oe, the $\chi_M(T,H)$ curves remain unchanged and the peaks for all of the curves appear at 3.0

(37) Engelfriet, D. W.; Groeneveld, W. L.; Groenendijk, H. A.; Smit, J. J.; Nap, G. M. *Z. Naturforsch.* **1980**, *35a*, 115.

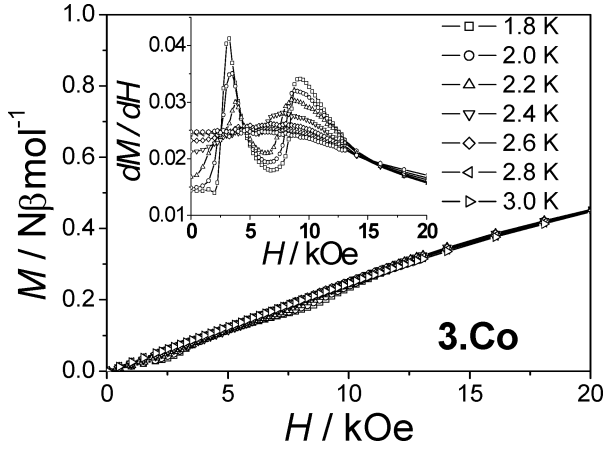

Figure 11. The isothermal magnetization of **3·Co** from 0 to 20 kOe at different temperatures from 1.8 to 3.0 K with a step of 0.2 K. Inset: the differentiate of $M(T,H)$ curves, dM/dH.

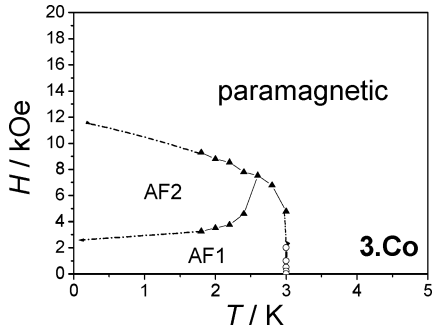

Figure 12. The proposed phase diagram in $H-T$ form for **3·Co**. The triangles and the circles represent the experimental data obtained from two different methods mentioned in the text, and the dashes were added artificially.

K, indicating the unique phase in the low-field range. Following these data, a possible simplified phase diagram of **3·Co** was proposed and shown in Figure 12. The triangular experimental points were obtained from the peaks in dM/dH versus H curves, the circles were obtained from the peaks of $\chi_M(T,H)$, and the dashed curves were added subjectively. From the phase diagram, we can see that the Néel temperature is 3.0 K, consistent with the ac susceptibility measurement. With increasing fields at low temperatures, **3·Co** transfers from one antiferromagnetic phase (AF1) to another one (AF2) and finally to the paramagnetic one. This kind of phase diagram is very similar to those with a field-induced spin-flop phase transition, which was found for many antiferromagnetic systems with weak anisotropy, commonly for Mn^{2+}, for example, because the spin-flop phase does not appear in a system with large anisotropy such as the Ising mode.[15b] The reason and the nature of this kind of spin-flop-like phase transition are not entirely understood; it might arise from the competitive antiferromagnetic interactions intra- and interchains via formate and 4,4′-bpy, respectively. Furthermore, the magnetic anisotropy of the single Co^{2+} ion and the twist of the adjacent coordination polyhedra of Co^{2+} ions make the situation even more complicated. A similar two-step transition was observed in other Co^{2+} compounds.[38]

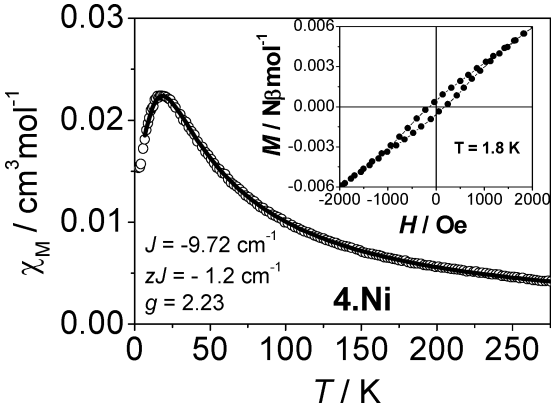

Figure 13. Temperature dependence of χ_M of **4·Ni** at $H = 30$ kOe from 2 to 275 K; the line presents the best fitting with the model discussed in the text. Inset: hysteresis loop for **4·Ni** at 1.8 K.

Experiments carried out on oriented single crystals are needed to further understand the magnetic property of **3·Co**.

4·Ni. The temperature dependence of χ_M of **4·Ni** from 2 to 275 K shows a peak at ca. 17 K (Figure 13). Fitting the data above 50 K with the Curie−Weiss law, we find $C = 1.30$ cm^3 K mol^{-1} and a negative Weiss constant $\theta = -29.9$ K (Figure S6), which indicates the dominant antiferromagnetic coupling between Ni^{2+} ions. Considering its structure, we use the analytical expression for an antiferromagnetic chain of $S = 1$ developed by C. Y. Weng[15a,39] with the Hamiltonian $H = -2J\sum_{\langle i,j\rangle}S_i \cdot S_j$,

$$\chi_{\text{chain}} = \frac{Ng^2\beta^2}{kT}\frac{2.0 + 0.0194x + 0.777x^2}{3.0 + 4.346x + 3.232x^2 + 5.834x^3} \quad (5)$$

with $x = |J|/kT$. J is the coupling of the neighboring Ni^{2+} bridged by *anti*−*anti* $HCOO^-$. Similar to **2·Co**, we use the molecular field approach eq 4 to fit the χ_M data, where χ_{mono} was replaced by χ_{chain} in eq 5 and zJ represents the summation of the coupling transferred by 4,4′-bpy and dipole−dipole interactions by considering those as the effect of molecular field. The best fitting gives $J = -9.7$ cm^{-1} $= -14.0$ K, $zJ = -1.2$ cm^{-1} $= -1.73$ K and $g = 2.23$ with $R = 4.4 \times 10^{-5}$ [$R = [\sum(\chi_{\text{obs}} - \chi_{\text{calc}})^2/\sum(\chi_{\text{obs}})^2]$]. These results indicate that **4·Ni** behaves as an antiferromagnetic-coupled chain.

Both ZFCM and FCM in 200 Oe from 2 to 40 K increase abruptly at ca. 21 K and diverge at 14.7 K (Figure 14). This behavior might come from the onset of long-range order. The in-phase ac susceptibility χ'_M in $H_{ac} = 3$ Oe and $H_{dc} = 0$ Oe shows a peak at 20 K, consistent with the peak of d(χ_M)/dT (Figure S9). No resolving out-of-phase signal and frequency dependence (selected frequency: 277, 666, 1633 Hz) were observed. The isothermal magnetization $M(T,H)$ increases almost linearly from 0 to 50 kOe, and then increases faster up to 70 kOe and reaches 0.22 μ_B per Ni^{2+} in 70 kOe (Figure S10), far from the saturation value $M_S = 1$ μ_B for a spin-only Ni^{2+} ion, indicating the strong antiferromagnetic coupling between Ni^{2+} ions. At 1.8 K, a hysteresis loop was observed with the remnant magnetization $M_R = 0.00035$ μ_B

(38) Yin, P.; Gao, S.; Zheng, L.-M.; Wang, Z.-M.; Xin, X.-Q. *Chem. Commun.* **2003**, 1076−1077.

(39) (a) Weng, C. Y. Ph.D. Thesis, Carnegie Institute of Technology, USA, 1968. (b) Hiller, W.; Strahle, J.; Datz, A.; Hanack, M.; Hatfield, W. E.; ter Haar, L. W.; Guetlich, P. *J. Am. Chem. Soc.* **1984**, *106*, 329.

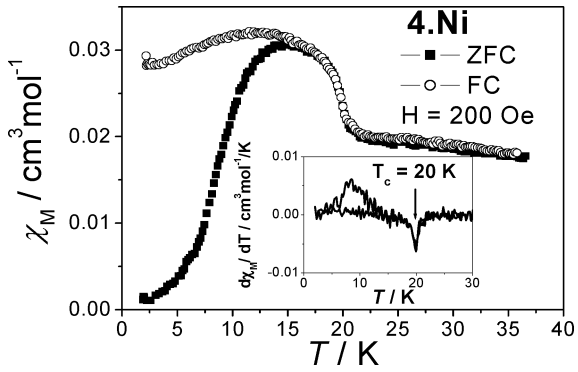

Figure 14. ZFCM and FCM of **4·Ni** in an external field of 200 Oe. Inset: the differentiate of ZFCM and FCM, $d\chi_M/dT$.

and the coercivity field $H_C \approx 200$ Oe (inset of Figure 13). Based on all of these results, **4·Ni** is a weak ferromagnet below 20 K due to antiferromagnetic interaction and spin-canting. The canting angle is very small and estimated to be 0.02°. The absence of an inversion center of the three-atom bridge μ-$HCOO^-$ and the noncentrosymmetric character of the structure may prefer the D−M interaction and lead to the spin-canting.

The magnetic properties of **2**−**4** differ much from those of the azide analogues. It is obvious considering their structural differences. Now, we can clearly see the similarity and the difference of formate and azide. The similarity includes the coordination mode, the negative charge, and the ability to mediate magnetic interactions. On the other hand, there exist great differences between them, including the strength of the transmitted magnetic interaction, the geometries, and the coordination abilities of O/N atoms. By considering the similarity of azide and formate, we may easily obtain new compounds by replacing one with the other, with the experimental conditions being considered carefully. Utilizing the differences between them, with various, practical experimental conditions, many new compounds with special structures and properties could be obtained. We are now investigating formate and azide compounds systemically by adding various secondary ligands. Some other new compounds with interesting magnetic properties were synthesized and will be reported in the future.

Conclusion

The formate anion, $HCOO^-$, is a suitable analogue of azide with which to construct molecule-based magnetic materials. By using formate and 4,4′-bpy as ligands, we successfully synthesized four formate compounds formulated as $M(HCOO)_2$(4,4′-bpy)·nH_2O (M = Mn, Co (**1·Mn**, **2·Co**), $n = 0$; M = Co, Ni (**3·Co**, **4·Ni**), $n = 5$). **1·Mn** and **2·Co** are both crystallized as a chiral 3D diamondoid structure bridged by *anti*−*anti* formate, like the azide analogue $Mn(N_3)_2$(4,4′-bpy). Both of them are weak ferromagnets below the critical temperatures $T_c = 5.3$ and 7.4 K, respectively. The weak ferromagnetism may originate from the D−M interaction between the adjacent metal ions bridged by the noncentrosymmetric formate. **3·Co** and **4·Ni** are both in a noncentrosymmetric noninterpenetrated $CdSO_4$ structure with channels along the *c*-axis. Residing in these channels, water molecules form novel T5(1) tapes constructed by vertex-sharing cyclic pentamers. **3·Co** is an antiferromagnet below 3.0 K, and **4·Ni** behaves as a weak ferromagnet below 20 K. Below 3 K, **3·Co** has a field-induced spin-flop-like transition, and a possible phase diagram is proposed in $H-T$ form. Also, using DFT calculations on the simplified models, we compared *anti*−*anti* formate with μ-1,3-azide for efficiency to mediate magnetic coupling. Our results show the similarities and the differences between formate and azide and offer a promising method for the design of new molecular architectures with these two important bridges.

Acknowledgment. We acknowledge support from the National Science Fund for Distinguished Young Scholars (20125104), NSFC Nos. 20490210, 20221101, and 90201014, and the Research Fund for the Doctoral Program of Higher Education (20010001020).

Supporting Information Available: CIF files of **1**−**4**, TGA data of **3** and **4**, plots of $\chi_M T(T)$ and $\chi_M^{-1}(T)$ for **1**−**4**, the derivative of ZFCM $d\chi_M/dT$ for **1**, $M(T,H)$ of **1** and **4**, ac isothermal magnetization and dM/dH of **3**, and ac magnetic susceptibilities of **2** and **4**. This material is available free of charge via the Internet at http://pubs.acs.org.

IC049170T